# Letters

## Mixed Resonant Frequency Control Improving Light-Load Efficiency of Full-Bridge LLC Converter

Jong-Woo Kim, *Member, IEEE*

***Abstract*—This letter introduces a mixed resonant frequency control improving the light-load efficiency of a full-bridge *LLC* converter. The proposed control significantly decreases the switching frequency under light-load condition, by inserting the subresonant freewheeling period caused by the magnetizing inductor of the transformer. By doing so, the operation of *LLC* converter becomes like a continuously operating burst mode, increasing the effective loading current. The advantages of the proposed control distinguished from the previous approaches are simple implementation, less switching losses, and zero impact on the dynamics. The effectiveness of the proposed control is verified through a prototype converter with a 400–300 V input and a 50 V/10 A output.**

***Index Terms*—Burst mode, efficiency, light load, *LLC* converter.**

### I. Introduction

In DATA center applications, the energy conversion efficiency under light-load conditions is getting more important [1]. This is because the data center spends a long time in the light-load conditions, especially during nighttime when user traffic is minimal.

*LLC* converter in Fig. 1 is the most famous converter topology in data center applications nowadays, due to its high efficiency with less components [2], [3], [4], [5]. *LLC* converter has a constant input voltage in the nominal state, following power factor correction circuit. The turns ratio of the transformer is the ratio of the input voltage to the output voltage ($n = V_{IN}/V_{OUT}$). By doing so, *LLC* converter operates around the resonant frequency in the entire load conditions. However, the constant switching frequency causes a fixed transformer core loss, deteriorating the efficiency in the light load conditions where the conduction loss is minimized.

The traditional approach to enhancing efficiency in a light-load condition is the burst mode control [6], [7]. This method involves cycling the *LLC* converter ON and OFF over a long period. By doing so, the *LLC* converter operates under heavier loading conditions where the efficiency is higher, eliminating losses during the OFF period. However, burst mode control often exhibits a poor dynamic response during transitions from light to heavy load conditions. Exiting burst mode during such transitions can resemble starting up under heavy load conditions. Optimized control strategies based on the state trajectory control can improve the dynamics [8], [9], but it still shows limitation and requires a complex analysis/control.

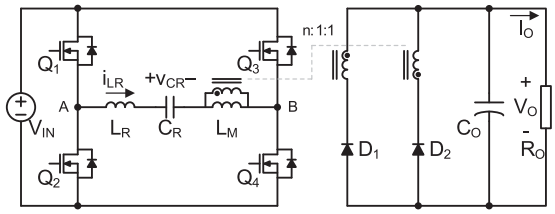


Fig. 1. *LLC* converter.

Pulsewidth modulation (PWM) control offers [10], [11], [12] a solution to improve light-load conditions without the dynamics problem. It applies asymmetric or phase-shifted gate signals to reduce the maximum flux density and switching frequency of the *LLC* converter. However, PWM control causes the distortion of the resonant current, leading to increased turn OFF losses and maximum flux density in the resonant inductor. Also, *LLC* converter still operates around the resonant frequency, having substantial core losses from the magnetic components.

Minimizing circulating currents [13], [14] also helps increase the efficiency of *LLC* and series resonant converter in the light load conditions. However, those methods require additional components [13], or the use of active components in the secondary side rectifier [14] to achieve less circulating current.

### II. Mixed Resonant Frequency Control

#### A. Operation Under a Light-Load Condition

Figs. 2 and 3 show the key waveforms and current paths of *LLC* converter with the mixed resonant frequency control (MRFC) under a light-load condition.

During $t_0 \sim t_1$, $Q_1$ and $Q_4$ are turned ON, and $v_{AB}$ becomes $V_{IN}$. $Q_1$ is turned ON during a half resonant period of $L_R$ and $C_R$

$$\frac{T_S}{2} \cong \pi\sqrt{L_R C_R}. \tag{1}$$

$L_R$ and $C_R$ resonate, and the difference between the resonant current $i_{LR}$ and $i_{LM}$ is delivered to the output side through the

Manuscript received 10 February 2024; revised 17 March 2024; accepted 5 April 2024. Date of publication 24 April 2024; date of current version 20 June 2024. This work was supported by the National Research Foundation of Korea (NRF) grant funded by the Korea government (MSIT) (No. RS-2024-00356482).

The author is with the Electrical and Electronics Engineering, Konkuk University, Gwangjin-Gu 05029, South Korea (e-mail: jongwookim@konkuk.ac.kr).

Color versions of one or more figures in this article are available at https://doi.org/10.1109/TPEL.2024.3392870.

Digital Object Identifier 10.1109/TPEL.2024.3392870

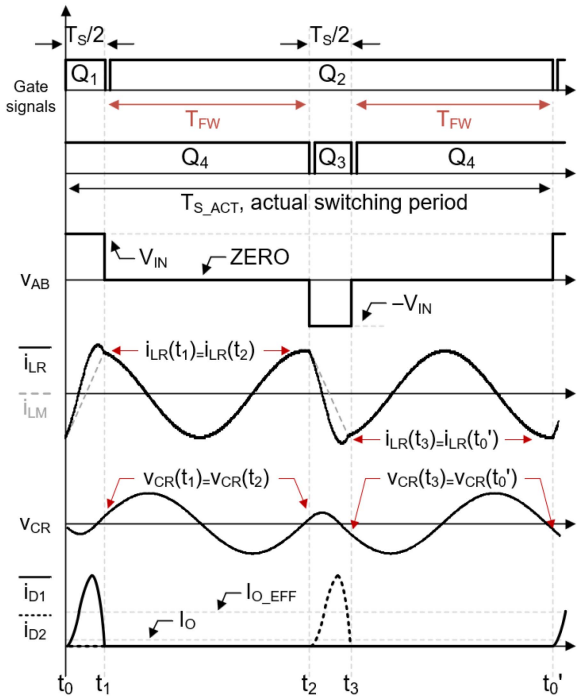


Fig. 2. Key waveforms of *LLC* converter with the MRFC under a light-load condition.

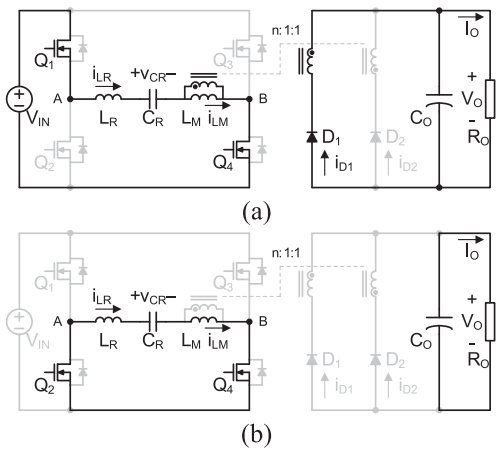


Fig. 3. Current paths of *LLC* converter with MRFC during (a) $t_0 \sim t_1$ and (b) $t_1 \sim t_2$.

transformer and rectifier diode $D_1$. The magnetizing current of the transformer $i_{LM}$ increases linearly. $Q_1$ is turned OFF at $t_1$. Since $i_{LR}$ becomes the same with $i_{LM}$ at $t_1$, $D_1$ is softly turned OFF. By having $T_S$ around the resonant period, the voltage conversion ratio of *LLC* converter still maintains around 1/n.

During $t_1 \sim t_2$, MRFC inserts a freewheeling period. $Q_1$ is OFF and $Q_2$ is turned ON. However, $Q_4$ is still turned ON so that $v_{AB}$ becomes zero. Since $D_1$ is turned OFF, $C_R$ resonates with series connected $L_M$ and $L_R$. The inserted freewheeling period $T_{FW}$ is the resonant period, so that the state variables ($i_{LM}$, $i_{LR}$, and $v_{CR}$) become identical at $t_1$ and $t_2$ as follows:

$$T_{FW} = 2\pi\sqrt{(L_M + L_R)\,C_R} \tag{2}$$

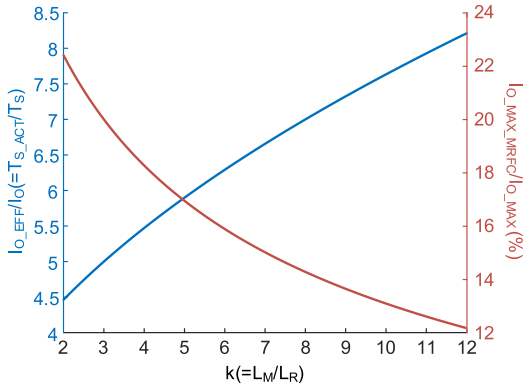


Fig. 4. $I_{O\_EFF}/I_O (= T_{S\_ACT}/T_S)$ and $I_{O\_MAX\_MRFC}/I_{O\_MAX}$ according to $k (= L_M/L_R)$.

$$i_{LR}\ (t_1) = i_{LR}\ (t_2) \tag{3}$$

$$v_{CR}\ (t_1) = v_{CR}\ (t_2)\,. \tag{4}$$

At $t_2$, $Q_4$ is turned OFF and $Q_3$ is turned ON. $Q_2$ and $Q_3$ are turned ON, and $v_{AB}$ becomes $-V_{IN}$. The operation in the remaining switching is symmetric with the operation during $t_0 \sim t_2$. The actual switching period with MRFC $T_{S\_ACT}$ can be found as follows:

$$T_{S\_ACT} = T_S + 2T_{FW}. \tag{5}$$

### B. Effective Load Current Under MRFC

The output charges provided during $t_0 \sim t_1$ and $t_2 \sim t_3$ cover all amount of the charges for the load. This makes *LLC* converter effectively operates under a heavier loading condition during $t_0 \sim t_1$ and $t_2 \sim t_3$. The relationship between the effective output current with MRFC ($I_{O\_EFF}$) and the actual output current ($I_O$) can be expressed as follows:

$$I_{O\_EFF}\ T_S = I_O\ T_{S\_ACT}. \tag{6}$$

Rearranging (1), (2), (5), and (6) provides a better understanding on the effective output current and the actual switching period of *LLC* converter under MRFC as follows:

$$\frac{I_{O\_EFF}}{I_O} = \frac{T_{S\_ACT}}{T_S} \cong \left[1 + 2\sqrt{1 + \frac{L_M}{L_R}}\right] = \frac{R_O}{R_{O\_EFF}} \tag{7}$$

where $R_{O\_EFF}$ represents the effective output resistance.

MRFC increases the effective loading condition, so it is required to limit $I_{O\_EFF}$ not to exceed the rated output current $I_{O\_MAX}$. From (7), the relationship between the maximum loading condition that MRFC is applicable ($I_{O\_MAX\_MRFC}$) can be obtained as follows:

$$I_{O\_MAX\_MRFC} = \frac{1}{1 + 2\sqrt{1 + \frac{L_M}{L_R}}}\ I_{O\_MAX}. \tag{8}$$

Fig. 4 represents $I_{O\_EFF}/I_O$ and $I_{O\_MAX\_MRFC}/I_{O\_MAX}$ according to k. Considering $L_M/L_R$ ratio of an *LLC* converter is designed to be 3–10 in most applications, the effective output current of an *LLC* converter with MRFC is 5–8 times of the

TABLE I
COMPONENTS LIST OF THE PROTOTYPE CONVERTER

| Item | Details | |
|---|---|---|
| Specification | $V_{IN}$: 400 (nominal) –300 V, $V_O$: 50 V, $I_O$: 10 A | |
| Main transformer T | PQ3535 N95 core n:1:1=40:5:5 | pri: 0.1Φx50 litz wire sec: 0.1Φx100 litz wire $L_M$=550 μH, $L_{LKG}$=19 μH |
| $Q_1$~$Q_4$ | IPW60R070C6 (600 V, 70 mΩ) | |
| $D_1$ and $D_2$ | FDH055N15A (150 V, 5.9 mΩ) | |
| $C_R$ | 44 nF (630 V 22 nF MLCC 2 EA) | |
| $L_R$ | 47 μH, RM8 N95 core (0.1 Φx50 litz wire 12 turns) | |
| $C_O$ | 1.32 mF (100 V 330μF electrolytic cap. 4 EA) | |
| Controller | TMS320F28049 from Texas Instruments | |

actual output current. Also, MRFC is applicable up to 13%–20% loading conditions.

### C. Voltage Conversion Ratio Under MRFC

According to the analysis in Section A, it can be noted that there is no change on the state variables between before/after the freewheeling period as follows:

$$i_{LR}\ (t_1) = i_{LR}\ (t_2) = -i_{LR}\ (t_3) = -i_{LR}\ (t_0') \tag{9}$$

$$v_{CR}\ (t_1) = v_{CR}\ (t_2) = -v_{CR}\ (t_3) = -v_{CR}\ (t_0')\,. \tag{10}$$

During the freewheeling period, *LLC* converter can be considered in an idle state. *After the freewheeling period, the LLC converter resumes operation with the same state variables as before the freewheeling.* It can be inferred that the operation during $t_0$~$t_1$ and $t_2$~$t_3$ is identical to that of the frequency-controlled *LLC* converter. Accordingly, the voltage conversion ratio of an *LLC* converter under MRFC can be obtained using the effective output resistance $R_{O\_EFF}$ and the first harmonic approximation as follows:

$$\frac{V_O}{V_{IN}} = \frac{1}{n\sqrt{\left[1+\frac{1}{k}\left\{1-\left(\frac{F_R}{F_S}\right)^2\right\}\right]^2 + \left[\frac{\pi^2 Q}{8n^2}\left(\frac{F_S}{F_R}-\frac{F_R}{F_S}\right)\right]^2}} \tag{11}$$

where $k = L_M/L_R$, $F_R = 1/2\pi\sqrt{L_R C_R}$, $F_S = 1/T_S$, and $Q = \frac{1}{R_{O\_EFF}}\sqrt{\frac{L_R}{C_R}}$. To have 1/n of the voltage conversion ratio, $F_S$ of an *LLC* converter under MRFC needs to be $F_R$. Therefore, $F_S$ of an *LLC* converter remains same as $F_R$ regardless of whether MRFC is applied or not. This contributes to the superior dynamic performance of MRFC, as it does not vary the output voltage at the moment of activation and deactivation.

## III. EXPERIMENTAL RESULTS

MRFC has been verified by a prototype converter with 400–300 V input and 50 V/10 A output. This specification is for the data center applications, where the input voltage is constant as 400 V in the nominal state and it decreases down to 300 V during the hold-up time [5]. Table I represents the components list of the prototype converter. $k(=L_M/L_R)$ is around 8.33, so $I_{O\_MAX\_MRFC}$ is around 14% loading condition.

Fig. 5 represents the implementation of MRFC. The implementation can be simply done by adding $T_{FW}$ block to the conventional pulse frequency control. In $T_{FW}$ block, a hysteresis is applied to prevent continuous mode change at the boundary. The exiting load current of MRFC can be determined considering (8) and the efficiency in the light load conditions. In this example, $I_{O\_MAX\_MRFC}$ is around 14% loading condition according to (8). Proposed MRFC can provide precise $V_O$ control although tolerance on the resonant tank exists, because proportional-integral controller adjusts $T_S$.

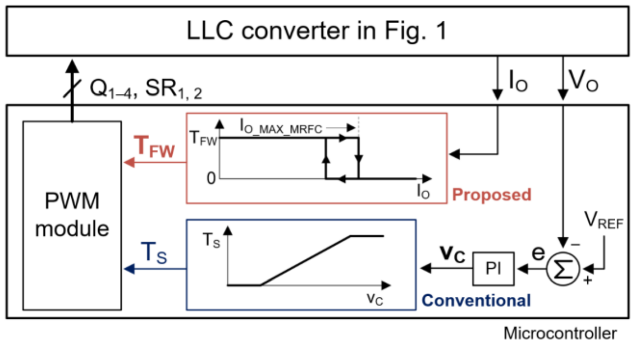


Fig. 5. Implementation of MRFC.

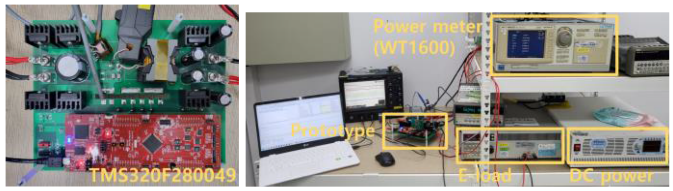


(a) (b)

Fig. 6. (a) Prototype converter. (b) Experimental setup.

Fig. 6 represents the prototype converter and the experimental setup. Microcontroller TMS320F280049 from Texas Instruments is selected for the implementation of MRFC. E-load is used for the load transient, and power meter WT1600 from Yokogawa is used to measure the efficiency.

Fig. 7(a) presents the experimental waveforms of the prototype converter with MRFC at $I_{O\_MAX\_MRFC}$ (15% load). The resonant frequency of $L_R$ and $C_R$ is around 100 kHz, so $T_S$ is around 10 $\mu$s to achieve 1/n voltage conversion ratio. At the beginning of the switching period, $Q_1$ is turned ON by $T_S/2$. After that, since the resonant frequency of $L_M$+$L_R$ and $C_R$ is around 30.5 kHz, 33 $\mu$s of $T_{FW}$ is inserted. It can be observed that the values of $i_{LR}$ before and after $T_{FW}$ are identical, indicating that there is no impact on the voltage conversion ratio caused by MRFC. $T_{S\_ACT}$ becomes around 76 $\mu$s, and the actual operating frequency is reduced to around 13.2 kHz, decreased by 7.6 times to conventional frequency control. At this point, the effective output current becomes the rated output current, therefore MRFC needs to be removed in heavier than $I_{O\_MAX\_MRFC}$ load current conditions to avoid excessive current stress and flux density on the components.

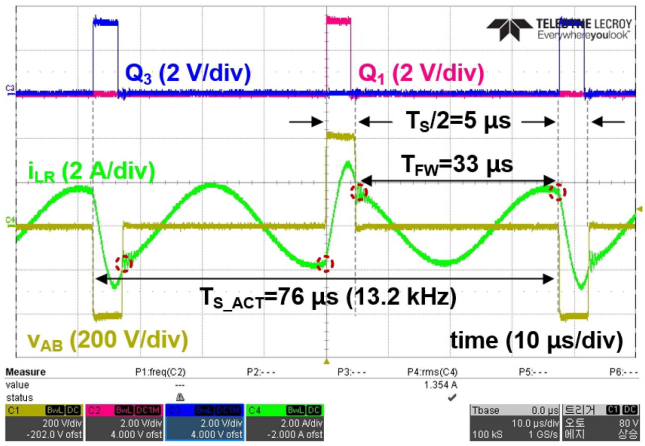


(a)

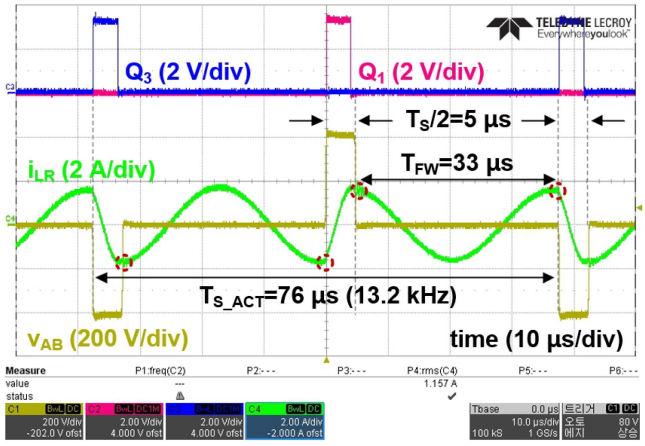


(b)

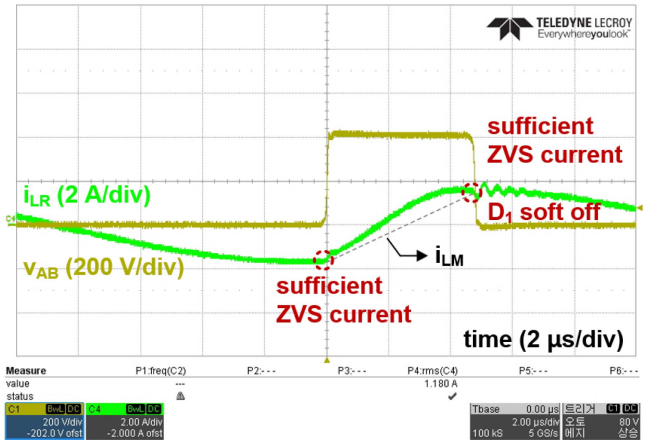


(c)

Fig. 7. Experimental waveforms of the prototype converter with MRFC at 400 V input and 50 V output conditions. (a) 1.5 A output ($I_{O\_MAX\_MRFC}$). (b) 0.5 A output. (c) Soft-switching zoomed in waveforms at 0.5 A output.

Fig. 7(b) presents the experimental waveforms of the prototype converter at 5% load condition and the zoomed in waveforms. As discussed in (11), MRFC still provides the constant output voltage regardless of the loading conditions.

Fig. 7(c) presents the zoomed in waveforms at 5% load condition. All primary side switches have sufficient zero voltage switching current, and the rectifier diodes are softly turned OFF. Therefore, due to the low frequency operation, soft switching, and minimized distortion on the resonant current, it can be inferred that MRFC substantially reduces the gate driving loss, switching loss and core losses from the magnetic components.

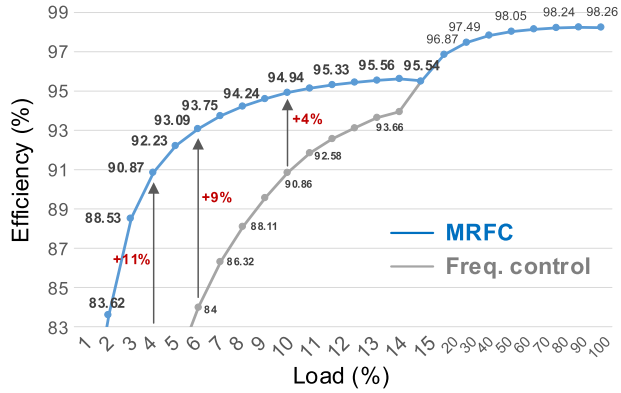


Fig. 8. Efficiency of the prototype converter (except for gate driving power).

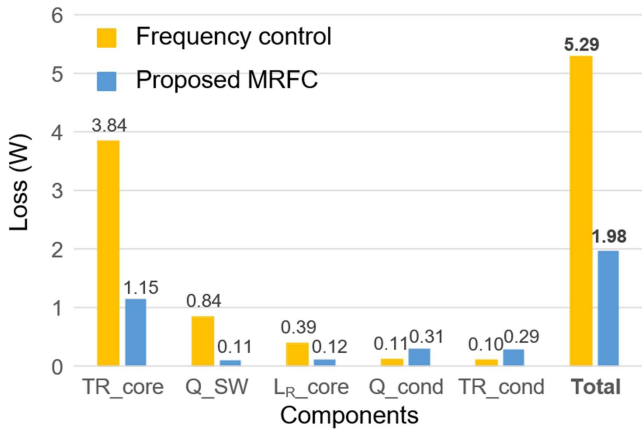


Fig. 9. Loss breakdown at 5% load condition.

Fig. 8 presents the efficiency of the prototype converter. Proposed MRFC achieves nearly 95% efficiency at 10% load condition, and it achieves even higher than 90% efficiency at 4% load condition.

Fig. 9 presents the loss breakdown at 5% load condition. As discussed, proposed MRFC significantly reduces the core losses and switching turn OFF losses which dominate the total loss in the light load conditions.

Fig. 10 presents the experimental waveforms under load transient conditions. Since MRFC does not affect the state variables at the switching moments of the primary side switches, it can achieve seamless kick-in or removal without affecting the output voltage regulation.

## IV. Further Discussions

### A. Maximum Flux Density on the Transformer

During the freewheeling period under MRFC, $C_R$ resonates with the series connected $L_M$ and $L_R$. Since $C_R$ and the inductors

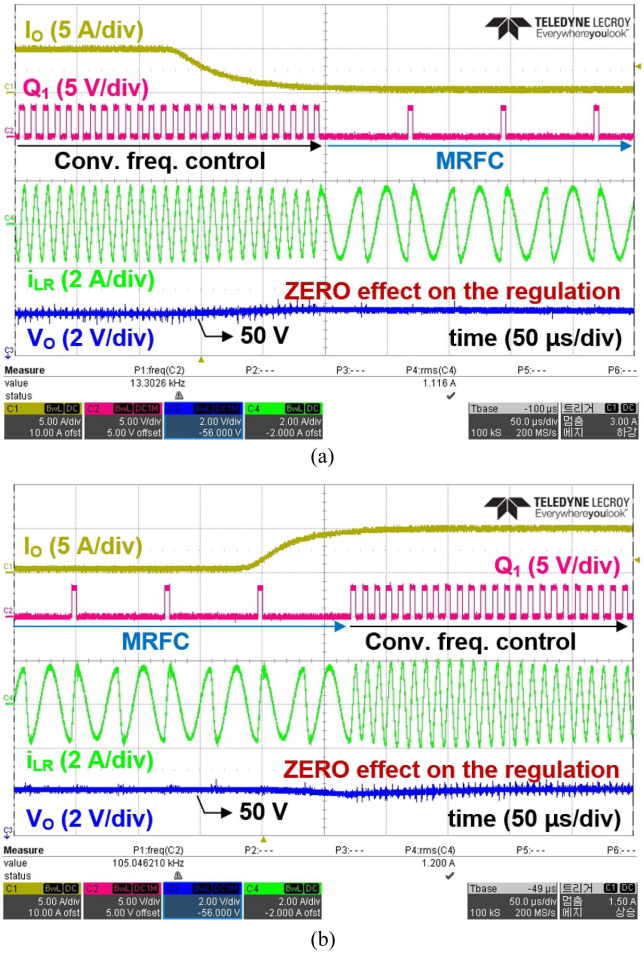


Fig. 10. Experimental waveforms under load transient (a) from 5% to 50% and (b) from 50% to 5%.

exchange their energy, the maximum resonant current during the freewheeling period ($I_{LR\_MAX\_FW}$) can be obtained from the following equation:

$$I_{\mathrm{LR\_MAX\_FW}} = \sqrt{i_{\mathrm{LR}}^2(t_1) + \frac{C_R}{L_{\mathrm{total}}} v_{\mathrm{CR}}^2(t_1)} \tag{12}$$

where $L_{total} = L_M + L_R$. Equation (12) mentions that the energy stored in $C_R$ at $t_1$ can increase the maximum current and also the maximum flux density on the main transformer. However, on the other hand, considering $L_{total} >> C_R$, MRFC does not increase the flux density significantly.

Considering the symmetricity of $i_{LR}$, $i_{LR}(t_1)$ can be obtained as follows:

$$i_{\mathrm{LR}}(t_1) = \frac{nV_O T_S}{4L_M}. \tag{13}$$

Also, considering the input current and the symmetricity of $v_{CR}$, $v_{CR}(t_1)$ can be obtained as follows:

$$v_{\mathrm{CR}}(t_1) = \frac{I_{\mathrm{O\_EFF}} T_S}{4nC_R}. \tag{14}$$

$v_{CR}(t_1)$ becomes the maximum when $I_{O\_EFF}$ is the rated output current. In the prototype converter, $i_{LR}(t_1) = 1.82$ A and $v_{CR}(t_1)$ $= 71$ V with $I_{O\_EFF} = 10$ A. According to (12), $I_{LR\_MAX\_FW}$ becomes 1.92 A, increased by 5%. It can be noted that the energy stored in the magnetic components is much larger than the energy stored in the resonant capacitor.

In the prototype converter, the maximum flux density of the transformer is increased from 0.111 to 0.117 T. On the other hand, the switching frequency is reduced from around 100 to 13 kHz concluding the proposed method reduces the core losses significantly in the light load conditions.

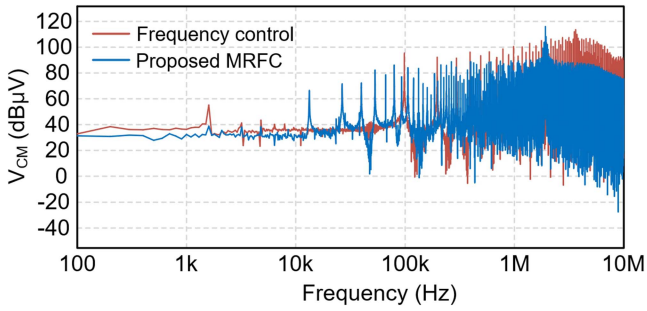


Fig. 11. CM noise comparison through simulation at 5% load.

### B. EMI and Audible Noise

Fig. 11 presents conducted CM noise comparison through simulation at 5% load condition. It can be noted that the proposed method shows quite similar noise level compared with the conventional frequency control, so the insertion loss during the filter design is not severely affected. Although the proposed control has noise in the audible band, the noise was not noticeable during the experiment. This is because small amount of energy circulates in a light load condition. Furthermore, designing the prototype converter for higher frequencies can shift the noise band above the audible range, mitigating potential noise issues.

### C. Gate Driving Loss

Since the proposed method achieves zero voltage switching without Miller plateau, gate driving loss ($P_{GD}$) of both the proposed MRFC can be obtained same as the conventional control as follows:

$$P_{\mathrm{GD}} = \left(4C_{\mathrm{iss\_Q}} + 2C_{\mathrm{iss\_SR}}\right) V_{\mathrm{DRV}}^2 f_{\mathrm{S\_ACT}} \tag{15}$$

where $C_{iss\_Q}$, $C_{iss\_SR}$, and $V_{DRV}$ present the total input capacitance of $Q_1$–$Q_4$, the total input capacitance of SR switches, and the switching frequency respectively. Since the proposed method reduces the switching frequency from 100 kHz to 13.2 kHz, it reduces $P_{GD}$ from 0.66 to 0.09 W, with $C_{iss\_Q} = 3.8$ nF, $C_{iss\_SR} = 7.1$ nF, and $V_{DRV} = 15$ V.

### D. Comparison With Prior Works

Table II presents the comparison of MRFC with state-of-the-art technologies. It can be noted that MRFC provides competitive advantages in terms of efficiency and dynamic performance.

TABLE II
COMPARISON WITH STATE-OF-THE-ART TECHNOLOGIES

| | Burst mode [9] | PWM [11] | Intermittent sinusoidal [14] | Proposed |
|---|---|---|---|---|
| Dynamics | Poor | Good | Good | Good |
| Switching | ZVS | ZVS | ZCS | ZVS |
| Switching frequency | Higher than $f_R$ | Around $f_R$ | Around $0.1*F_R$ | Around $0.13*f_R$ |
| Eff. at 10 % load | 92 % | 93.8 % | 95 % | 95 % |

## V. CONCLUSION

This letter proposes a MRFC, which substantially increases the light-load efficiency of a full-bridge *LLC* converter. By inserting a freewheeling period, which is the subresonant period caused by the magnetizing inductor, the proposed control reduces the actual operating frequency of *LLC* converter under light-load conditions. MRFC ensures the same voltage conversion ratio at the moment of activation and deactivation, enabling superior dynamic performance compared to conventional burst mode control. With its simplicity and robust performance, MRFC offers a practical solution for enhancing the energy efficiency of data centers.

## REFERENCES

[1] 80 Plus Power Supply Certification Program, May 16, 2024. [Online]. Available: https://www.clearesult.com/80plus/

[2] J.-W. Kim, M.-H. Park, B.-H. Lee, and J.-S. Lai, "Analysis and design of LLC converter considering output voltage regulation under no-load condition," *IEEE Trans. Power Electron.*, vol. 35, no. 1, pp. 522–534, Jan. 2020.

[3] J.-W. Kim and G.-W. Moon, "A new LLC series resonant converter with a narrow switching frequency variation and reduced conduction losses," *IEEE Trans. Power Electron.*, vol. 29, no. 8, pp. 4278–4287, Aug. 2014.

[4] J.-W. Kim, M. Lee, and J.-S. Lai, "Efficient LLC resonant converter with a simple hold-up time compensation in voltage doubler rectifier," *IEEE J. Emerg. Sel. Topics Power Electron.*, vol. 7, no. 2, pp. 843–850, Jun. 2019, doi: 10.1109/JESTPE.2019.2903192.

[5] J.-W. Kim, "LLC converter with hold-up time compensation using partial power process with semi-active bridge rectifier," *IEEE Trans. Power Electron.*, vol. 39, no. 5, pp. 5902–5912, May 2024.

[6] ON Semiconductor, Phoenix, AZ, "NCP1395 A/B: High performance resonant mode controller," Sep. 2008. [Online]. Available: https://www.onsemi.com/pdf/datasheet/ncp1395-d.pdf

[7] Texas Instruments, Dallas, "UCC25600: 8-pin high-performance resonant mode controller," Sep. 2008. [Online]. Available: https://www.ti.com/lit/ds/symlink/ucc25600.pdf

[8] W. Feng, F. C. Lee, and P. Mattavelli, "Optimal trajectory control of burst mode for LLC resonant converter," *IEEE Trans. Power Electron.*, vol. 28, no. 1, pp. 457–466, Jan. 2013.

[9] C. Fei, Q. Li, and F. C. Lee, "Digital implementation of light-load efficiency improvement for high-frequency LLC converters with simplified optimal trajectory control," *IEEE J. Emerg. Sel. Topics Power Electron.*, vol. 6, no. 4, pp. 1850–1859, Dec. 2018.

[10] J.-H. Kim, C.-E. Kim, J.-K. Kim, J.-B. Lee, and G.-W. Moon, "Analysis on load-adaptive phase-shift control for high efficiency full-bridge LLC resonant converter under light-load conditions," *IEEE Trans. Power Electron.*, vol. 31, no. 7, pp. 4942–4955, Jul. 2016.

[11] J.-W. Kim, J.-K. Han, and J.-S. Lai, "APWM adapted half-bridge LLC converter with voltage doubler rectifier for improving light load efficiency," *IET Electron. Lett.*, vol. 53, no. 5, pp. 339–341, May 2017.

[12] A. Awasthi, S. Bagawade, and P. K. Jain, "Analysis of a hybrid variable-frequency-duty-cycle-modulated low-Q LLC resonant converter for improving the light-load efficiency for a wide input voltage range," *IEEE Trans. Power Electron.*, vol. 36, no. 7, pp. 8476–8493, Jul. 2021.

[13] Y. Jeong, M.-S. Lee, J.-D. Park, J.-K. Kim, and R. A. L. Rorrer, "Hold-up time compensation circuit of half-bridge LLC resonant converter for high light-load efficiency," *IEEE Trans. Power Electron.*, vol. 35, no. 12, pp. 13126–13135, Dec. 2020.

[14] Z. Fang, H. Dong, H. Sun, F. Xie, and Z. Huang, "Intermittent sinusoidal modulation of bidirectional series resonant converter with zero current switching, linear current controllability, and load-independent efficiency," *IEEE Trans. Power Electron.*, vol. 37, no. 10, pp. 11725–11738, Oct. 2022.